Materials **2014**, *7*, 4105-4117; doi:10.3390/ma7064105

OPEN ACCESS

materials

ISSN 1996-1944

www.mdpi.com/journal/materials

Article

Biocompatibility and Surface Properties of TiO_2 Thin Films Deposited by DC Magnetron Sputtering

Francisco López-Huerta [1,*], Blanca Cervantes [1,2], Octavio González [2,3], Julián Hernández-Torres [1], Leandro García-González [1], Rosario Vega [2], Agustín L. Herrera-May [1] and Enrique Soto [2]

[1] Centro de Investigación en Micro y Nanotecnología, Universidad Veracruzana, Calzada Ruiz Cortines 455, 94294 Boca del Río, Veracruz, Mexico; E-Mails: blanca.cervantes@gmail.com (B.C.); julihernandez@uv.mx (J.H.-T.); leagarcia@uv.mx (L.G.-G.); leherrera@uv.mx (A.L.H.-M.)

[2] Instituto de Fisiología, Benemérita Universidad Autónoma de Puebla, Av. San Claudio 6301, Col. San Manuel, 72570 Puebla, Mexico; E-Mails: octavio.gp.21@gmail.com (O.G.); axolotl_56@yahoo.com.mx (R.V.); esoto24@gmail.com (E.S.)

[3] Licenciatura en Biomedicina, Benemérita Universidad Autónoma de Puebla, 13 Sur 2702, Col. Volcanes, 72410 Puebla, Mexico

* Author to whom correspondence should be addressed; E-Mail: frlopez@uv.mx; Tel.: +52-229-775-2000 (ext. 11956); Fax: +52-229-775-2000.

Received: 10 April 2014; in revised form: 1 May 2014 / Accepted: 5 May 2014 / Published: 27 May 2014

Abstract: We present the study of the biocompatibility and surface properties of titanium dioxide (TiO_2) thin films deposited by direct current magnetron sputtering. These films are deposited on a quartz substrate at room temperature and annealed with different temperatures (100, 300, 500, 800 and 1100 °C). The biocompatibility of the TiO_2 thin films is analyzed using primary cultures of dorsal root ganglion (DRG) of Wistar rats, whose neurons are incubated on the TiO_2 thin films and on a control substrate during 18 to 24 h. These neurons are activated by electrical stimuli and its ionic currents and action potential activity recorded. Through X-ray diffraction (XRD), the surface of TiO_2 thin films showed a good quality, homogeneity and roughness. The XRD results showed the anatase to rutile phase transition in TiO_2 thin films at temperatures between 500 and 1100 °C. This phase had a grain size from 15 to 38 nm, which allowed a suitable structural and crystal phase stability of the TiO_2 thin films for low and high temperature. The biocompatibility experiments of these films indicated that they were appropriated for culture of living neurons which displayed normal electrical behavior.

Keywords: biocompatibility; dorsal root ganglion neurons; direct current magnetron sputtering; thin film; TiO_2

1. Introduction

Recent advances in the complementary metal oxide semiconductor (CMOS) and micro-electro-mechanical systems (MEMS) technologies have allowed the fabrication of CMOS-MEMS devices that can be used on diverse areas such as agriculture, communications, environment, medicine and biomedical applications [1–5]. The biocompatibility is the capability of not to elicit a negative physiological response while maintaining functionality within the body environment [6,7]. Materials need to be screened and verified for their biocompatibility before use in living organism according with international norms [8]. Many of the materials implemented in CMOS-MEMS devices are opaque or dark, which causes problems to examine their biocompatibility using traditional methods [9]. One solution is to use a 3-(4,5-dimethyl-2-thiazolyl)-2,5-diphenyl-tetrazolium bromide (MTT) assay or to develop systems based on transparent material such as indium-tin oxide (ITO) and titanium dioxide (TiO_2) [10–13]. For instance, Titanium alloys are commonly employed to manufacture hard tissue replacement, including dental implants, bone plates and artificial hip joints [14–18]. These materials have positive characteristics such as good mechanical strength, lightweight, biocompatibility, and corrosion resistance, which generally depend of their surface properties [14,19].

TiO_2 films are an option for use in solar cells, photocatalysis, sensors, photoelectrolysis, biomedical devices, and biomaterials [20–25]. TiO_2 has three main polymorphic phases: rutile, anatase and brookite. Both anatase and rutile phases have tetragonal crystal structures but belong to different space groups. The low-density solid phases have less stability and undergo transition to rutile in the solid state. This phase transition is accelerated by heat treatment and can occur at temperatures between 450 and 1200 °C. It depends on the following parameters: initial particle size, initial phase, dopant concentration, reaction atmosphere and annealing temperature [26,27]. The TiO_2 films can be synthesized by different methods such as sol-gel, thermal spraying and physical vapor deposition [11,28–30]. In addition, the direct current (DC) reactive magnetron sputtering method is used to control the composition and structure of TiO_2 films, and it provides a strong substrate adhesion and large area with uniform thickness. This method can easily adjust the deposition conditions and offers a high deposition rate using argon gas, which is attractive for large-scale production. For biomedical applications, these films must have biocompatibility to avoid toxic effects on biological systems. Biocompatibility tests must evaluate the biomaterial cytotoxicity and the functionality of the biological system when it is exposed to this biomaterial [31–37]. Biocompatibility studies of an inorganic material require complex experiments both *in vitro* and *in vivo* in order to test the local and systemic effects of the material on cultured cells, tissue sections, and the whole body. *In vitro* cell culture tests are often used to screen the short term biocompatibility of inorganic material. These tests are sensitive, reliable, convenient, and reproducible screening methods. The study of the *in vitro* biocompatibility offers a controlled environment to test specific cellular and molecular processes. It

has less variability than the *in vivo* tests and facilitates the experimental replication. In order to use TiO_2 thin films in the biomedical microsensors fabrication, these films must satisfy the *in vitro* biocompatibility tests. Next, these microsensors must be satisfactory evaluated *in vivo* animals. Finally, they could be used in clinical studies. Thus, we present a biocompatibility analysis and surface characterization of TiO_2 thin films deposited on a quartz substrate, which are generated by reactive DC magnetron sputtering and annealing at different temperatures.

2. Results and Discussion

2.1. Physical Properties of the TiO_2 Films

The TiO_2 thin films are characterized using an X-ray diffractometer (XRD) at room temperature. The microstructural properties of the films were measurement using XRD (Bruker, D8 Advance, Karlsruhe, Germany) with CuKα radiation in the 2θ degree angle between 20° and 80°. Figure 1 shows the XRD data of TiO_2 thin films annealed to temperatures between 100 and 1100 °C. The X-ray diffraction pattern of the TiO_2 thin films shows a maximum signal about 20°, which is due to the quartz substrate. Similar X-ray diffraction patterns are obtained of TiO_2 thin films annealed between 100 and 300 °C. However, X-ray diffraction patterns of TiO_2 thin films annealed at 500 °C showed sharp diffraction peaks that can be assigned to the anatase TiO_2 phase with tetragonal body-centered structure (ICDD: 00-021-1272) [38].

Figure 1. X-ray diffraction patterns for films annealed at different temperatures.

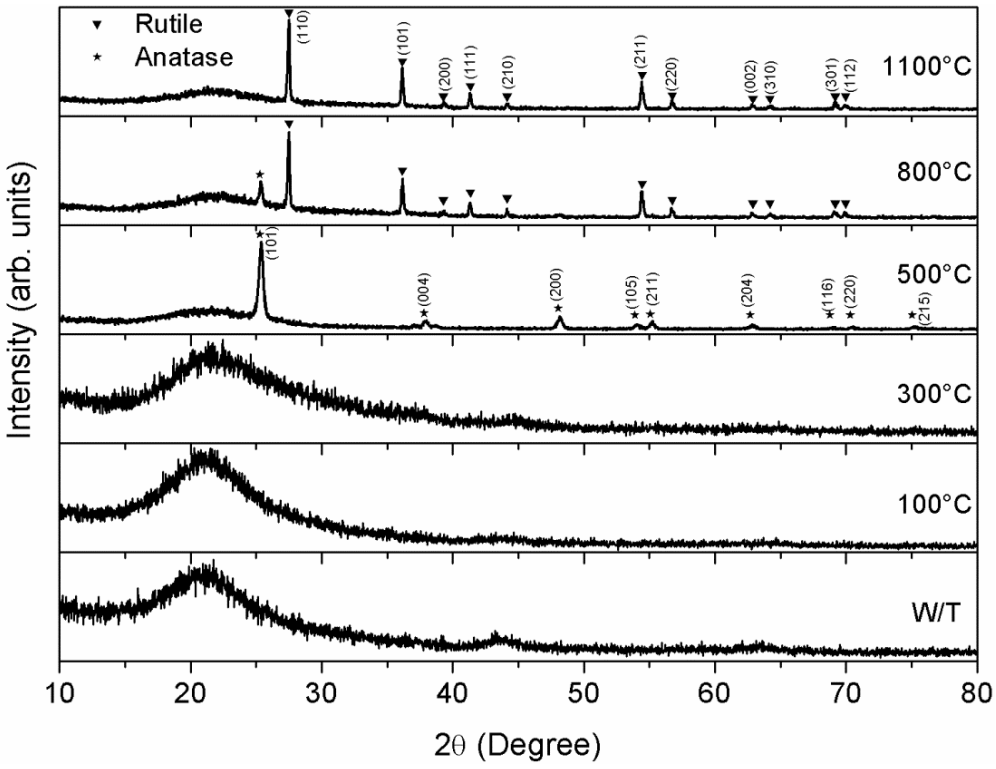

In addition, the X-ray diffraction pattern of the TiO_2 thin film annealed at 800 °C showed the coexistence of anatase-rutile, in where the intensity of rutile phase over anatase phase increased due to increment of the thermal annealing treatment. The rutile TiO_2 phase (ICDD: 01-089-4920) [39]

showed a tetragonal body-centered structure and a crystallographic orientation in plane (110). Finally, TiO_2 thin film annealed at 1100 °C had a set of sharp diffraction lines of the rutile TiO_2 phase. We conclude that the films have a strong orientation in the direction normal to the substrate surface.

The average crystalline grain size of anatase and rutile phase of TiO_2 thin films are shown in Table 1. The increment of the thermal annealing treatment caused that the grain size of the anatase and rutile TiO_2 phase had an increased and decreased, respectively. The crystalline grain size is obtained by the X-ray line profile analysis through of the Warren-Averbach method using a Pearson VII function (McKeehan) [40].

Table 1. Average values of the crystalline grain size of anatase and rutile phase TiO_2 films annealed at different temperatures.

Heat Treatment (°C)	Crystalline Size (nm)	
	Anatase TiO_2	Rutile TiO_2
500	15.9	–
800	20.8	37.5
1100	–	32.7

2.2. Biocompatibility Test

The control glass substrate and TiO_2 thin film surfaces of the neurons displayed typical membrane ionic currents activated by voltage variations, including a fast inward current at the beginning of voltage clamp pulse (Na^+ current) and ensuing outward currents (K^+ currents). This set of membrane ionic currents constitute the basis of the electrical excitability of neurons. The Na^+ current form the upstroke of the action potential and the ensuing K^+ currents repolarize the membrane (Figure 2A,C,E). The inward and outward current density of the dorsal root ganglion (DRG) neurons of Wistar rats cultured in the control substrate and TiO_2 thin films are evaluated. The current density is obtained dividing the current amplitude with respect to the membrane capacitance. The inward and outward current are measured at −20 and +40 mV, respectively.

The inward current density is significantly less for DRG neurons grown on the TiO_2 thin film surfaces prepared at room temperature and at 300 and 1100 °C than that for DRG neurons grown on the control substrate (Table 2 and Figure 3A). Regarding other TiO_2 thin films annealed at temperatures of 100, 500 and 800 °C, there is no significant difference compared with control substrate (Table 2 and Figure 3A). The amplitude of the outward current density of the DGR neurons cultured in the TiO_2 thin films surfaces at room temperature and 1100 °C are lower than those obtained for neurons cultured on the control substrate (Table 2 and Figure 3B). The outward current density in other TiO_2 thin films is not significantly different with respect those measured of the control substrate (Table 2 and Figure 3B).

In current clamp experiments, the membrane voltage of the cells is about −60 mV and under depolarizing current pulse injection, the DRG neurons are capable of firing typical action potentials of similar morphology both in control substrate and TiO_2 films surfaces (Figure 2B,D,F).

To analyze the properties of action potentials, we recorded the response to current pulses of DRG neurons grown on the control substrate and TiO_2 thin films surfaces (Figure 4). The most of the action potential parameters measured of the TiO_2 films surfaces are not significantly different from those

measured in the control substrate (Table 3). Only the action potential depolarization rate measured of the TiO_2 film surface annealed at 500 °C (n = 6) is significantly lower than that of the control substrate (Table 3; p = 0.039). In addition, the threshold of the TiO_2 films surfaces annealed at 100 and 500 °C are significantly lower than that of the control substrate (n = 5, p = 0.013 and n = 6, p = 0.017 respectively).

Figure 2. Representative membrane ionic currents and membrane voltage response of DRG neurons cultured in control substrate and TiO_2 thin films surfaces. (**A**,**C**,**E**) ionic currents generated with an 800 ms pulse (from −110 to +40 mV) followed by 200 ms test pulses to 0 mV (V_H = −60 mV). Neurons grown on control glass surface and those grown on TiO_2 films annealed at 100 and 800 °C showed similar set of currents with an initial rapid inward current followed by a slowly inactivating outward current; (**B**,**D**,**F**) representative voltage responses to current pulse injection (100, 400 and 300 pA, and V_m = −60 mV) of DRG neurons cultured in control substrate and TiO_2 thin films annealed at 100 and 800 °C. Recordings of the voltage response of neurons to a current pulse showed typical action potential discharge showing the functionality of the neurons growth in control and TiO_2 films.

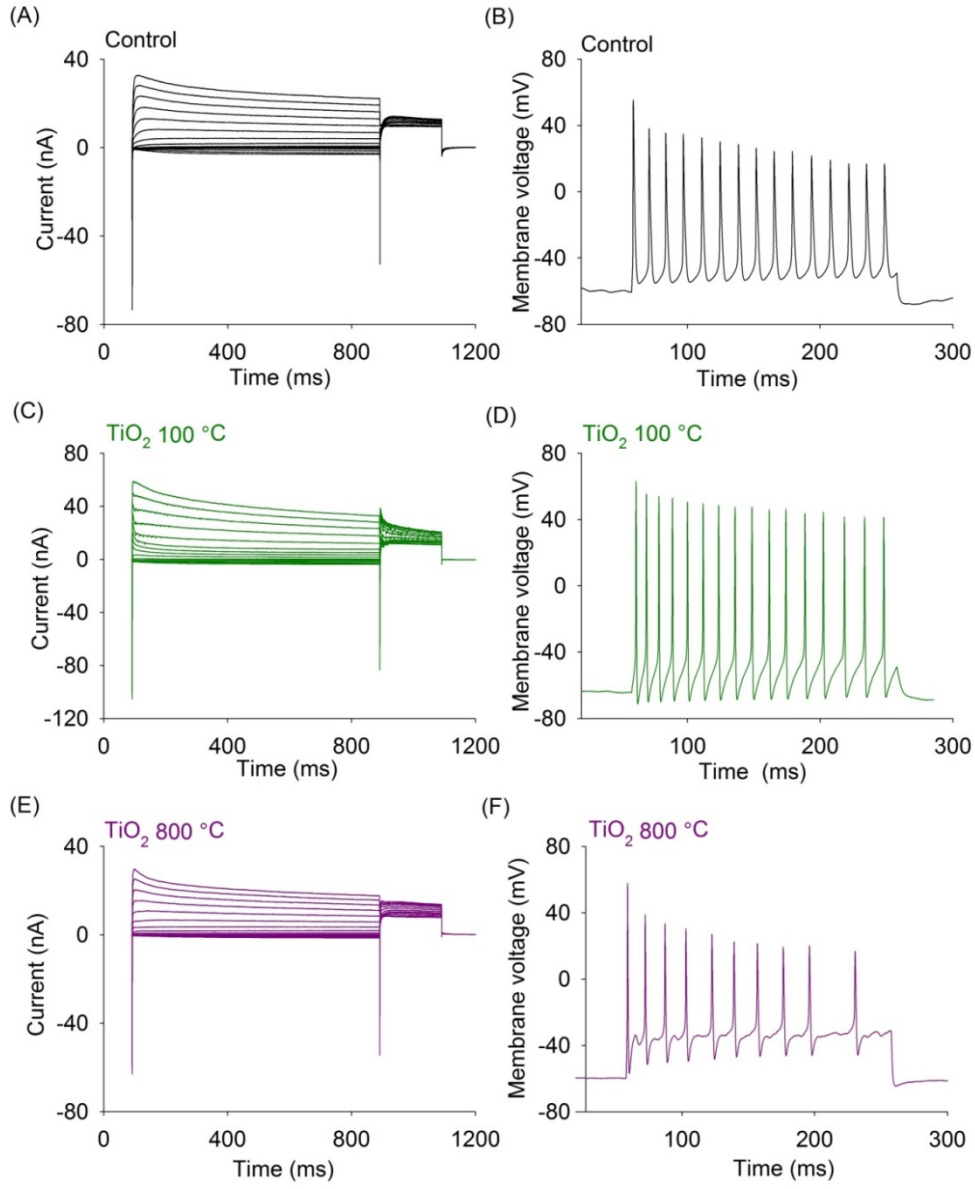

Table 2. Inward and outward current density in DRG neurons cultured in the control substrate and TiO_2 thin films surfaces prepared at room temperature and annealed at temperatures between 100 and 1100 °C.

Current Density	Control (n = 6)	TiO_2 Room Temperature (n = 7)	TiO_2 100 °C (n = 5)	TiO_2 300 °C (n = 6)	TiO_2 500 °C (n = 5)	TiO_2 800 °C (n = 5)	TiO_2 1100 °C (n = 9)
pA/pF inward current	−813 ± 195	−218 ± 98 * p = 0.016	−462 ± 208 p = 0.250	−276 ± 126* p = 0.043	−375 ± 178 p = 0.138	−715 ± 126 p = 0.695	−164 ± 62 * p = 0.003
pA/pF outward current	670 ± 121	285 ± 53 * p = 0.011	362 ± 79 p = 0.073	396 ± 103 p = 0.115	555 ± 103 p = 0.576	758 ± 107 p = 0.606	298 ± 54 * p = 0.012

Mean ± standard error, * $p < 0.05$.

Figure 3. Inward and outward current density of the DRG neurons cultured in control substrate and TiO_2 thin films. (**A**) Average inward current density as a function of voltage; (**B**) Average outward current density as a function of voltage.

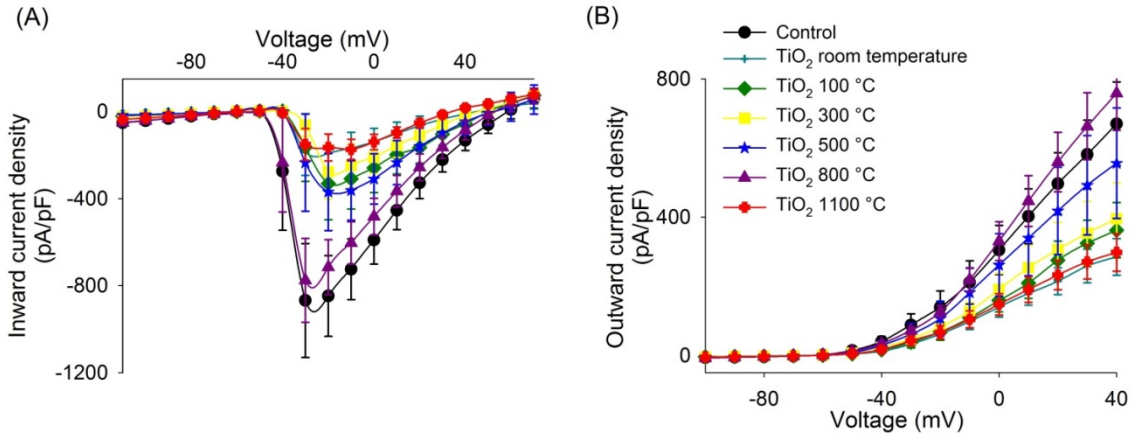

Figure 4. Representative action potential recordings of the DRG neurons on control substrate and TiO_2 thin films annealed at 1100 °C. (**A**) Action potential produced by a 100 pA depolarizing current pulse; (**B**) Phase-plane plot of the action potential shown in panel A. 1—AHP, 2—threshold, 3—maximum depolarization rate, 4—maximum repolarization rate; (**C**) Action potential caused by 100 pA depolarizing current pulse in a neuron cultured on the TiO_2 film; (**D**) Phase-plane plot for the action potential shown in panel C. 1—AHP, 2—threshold, 3—maximum depolarization rate, 4—maximum repolarization rate.

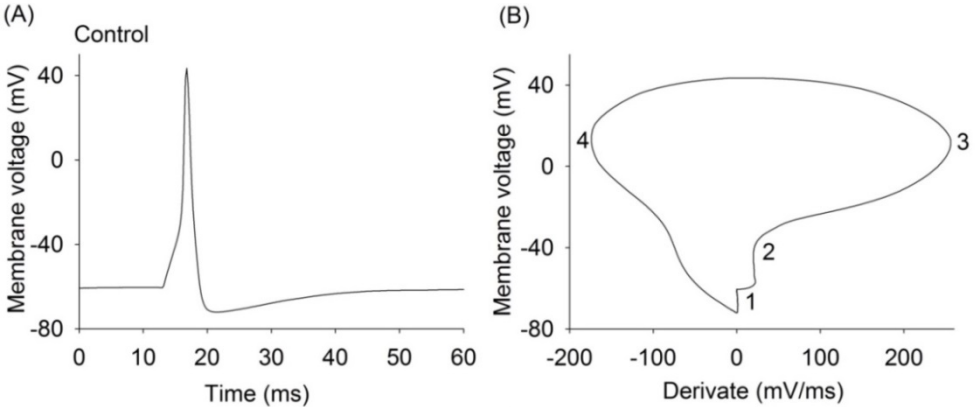

Figure 4. *Cont.*

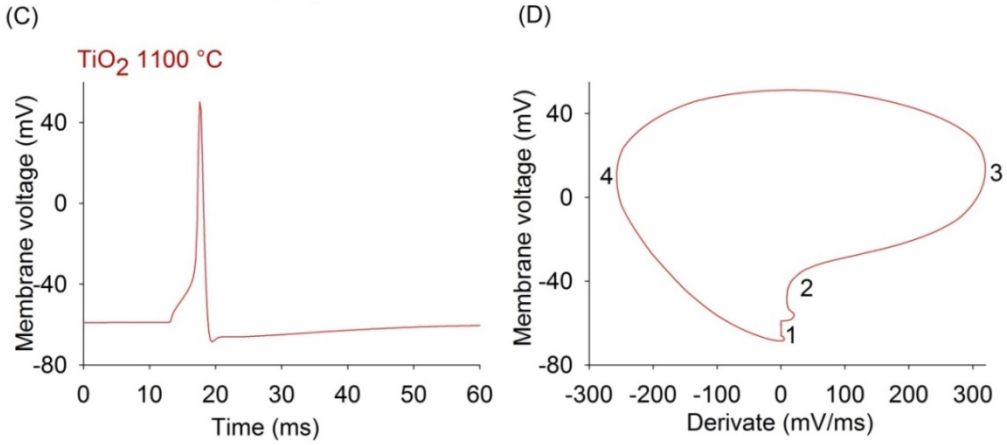

Table 3. Properties of action potentials of DRG neurons grown on control substrate and TiO_2 thin film.

Action Potential Parameters	Control (n = 7)	TiO_2 Room Temperature (n = 5)	TiO_2 100 °C (n = 5)	TiO_2 300 °C (n = 6)	TiO_2 500 °C (n = 6)	TiO_2 800 °C (n = 6)	TiO_2 1100 °C (n = 5)
Resting membrane potential	−60 ± 0.5	−62 ± 2	−62 ± 1	−60 ± 0.4	−61 ± 2	−60 ± 0.2	−60 ± 1
Amplitude of the action potential (mV)	109 ± 7	106 ± 8	113 ± 8	109 ± 5	104 ± 3	108 ± 9	95 ± 10
Duration 50% (ms)	1.2 ± 0.3	1.3 ± 0.3	0.81 ± 0.1	1.2 ± 0.2	2.3 ± 0.6	0.84 ± 0.1	1.1 ± 0.3
Maximum depolarization rate (mV/ms)	318 ± 42	236 ± 53	334 ± 59	253 ± 50	181 ± 39 *	311 ± 62	209 ± 66
Maximum repolarization rate (mV/ms)	−118 ± 23	−94 ± 17	−170 ± 17	−145 ± 21	−91 ± 37	−164 ± 23	−155 ± 40
Threshold (mV)	−36 ± 2	−34 ± 4	−24 ± 4 *	−30 ± 4	−23 ± 4 *	−34 ± 2	−32 ± 4
Amplitude of the AHP (mV)	−10 ± 2	−6 ± 2	−8.5 ± 1	−9 ± 1	−9 ± 2	−9 ± 0.4	−10 ±0.5

Mean ± standard error, * $p < 0.05$.

In the control glass substrate and TiO_2 films annealed at room temperature and 100 °C, the 37% of the DRG neurons produced repetitive firing when were subjected to depolarizing current pulse injection. In the other TiO_2 films only 33% of the DRG neurons produced two or more action potential.

3. Experimental Section

3.1. TiO_2 Films Deposition

TiO_2 thin films are deposited on a quartz substrate at room temperature by DC magnetron sputtering using a titanium target, which has a diameter of 50.8 mm. A TiO_2 ceramic material is located on a 20% of the titanium target surface, in which both materials registered a purity of 99.99%, respectively. First,

the quartz substrate is cleaned using ultrasonic baths of C_3H_6O, C_2H_6O, and distilled water during 5 min at room temperature. This procedure is repeated four times and, after, the TiO_2 thin films depositions are made under an Argon (Ar) atmosphere and a chamber pressure of 5.6×10^{-6} Torr. The Ar flow is kept to 15 standard cubic centimeters per minute (sccm) during the TiO_2 films deposition by DC magnetron sputtering. The DC power and substrate temperature are controlled to 100 W and 25 °C, respectively. Figure 5 shows a reactive DC magnetron-sputtering system, which is used to deposit TiO_2 thin films on a quartz substrate (25.4 mm × 25.4 mm). Next, TiO_2 films are subjected to thermal-annealing treatment to achieve their phase transformation. For this treatment, a thermo scientific thermolyne muffle furnace (model F48025-60-80, Thermo Fisher Scientific Inc., Waltham, MA, USA) is used to keep the temperature during one hour in each heat treatment. The time of each heat treatment is lower than that reported in elsewhere [40]. In addition, it is enough to reach the required recrystallization and transformation phases. Finally, TiO_2 thin films are annealed at different temperatures (100, 300, 500, 800 and 1100 °C) to the anatase-to-rutile phase transformation.

Figure 5. The parameters used in the deposition of TiO_2 thin films were: pressure 5.6×10^{-6} Torr, Ar flow 15 sccm, time 60 min, power 100 W and substrate temperature 25 °C.

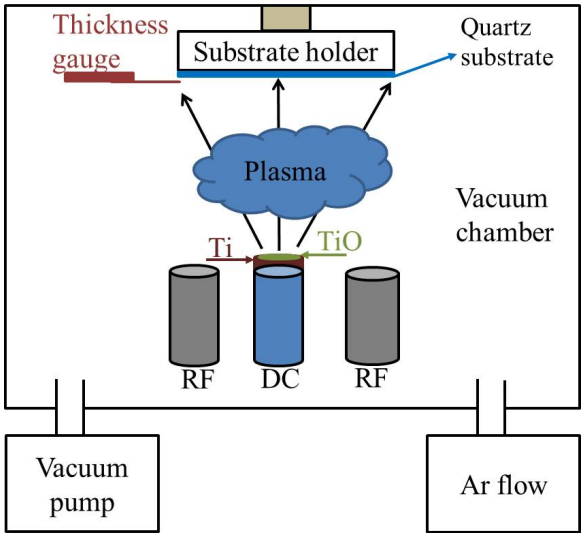

3.2. Cell Culture

Experimental procedures involving animals are reviewed and approved by the Institutional Animal Care and Use Committee (CICUAL) of Vice-rectory for Research and Graduate Studies of Autonomous University of Puebla (VIEP-BUAP). Animal care and experimental procedures are performed in accordance with Mexican national regulations on Animal Care and Experimentation (NOM-062-ZOO-1999) [41]. These regulations are made to minimize the animal suffering and to reduce the number of used animals, as outlined in the Guide to the Care and Use of Laboratory Animals of the National Academy of Sciences (NAS). For the cell culture, Wistar rats (P7-P10) are euthanized by decapitation and their dorsal root ganglia are isolated from the vertebral column. Next, the tissues of the dorsal root ganglia are incubated in culture medium L-15 (Gibco, Thermo Fisher Scientific Inc., Waltham, MA, USA) added with 0.125% collagenase and 0.125% trypsin during 30 min at 37 °C. The dorsal root ganglia are subsequently washed with L-15 medium, and dissociated by

mechanical agitation. In addition, dissociated cells are placed on both a control substrate (glass without TiO_2 films) and TiO_2 thin films, respectively, during a necessary time to allow the adherence of the cells with the TiO_2 surface. Later, fetal bovine serum (FBS) 10% (Gibco) and L-15 medium (modified for CO_2 by supplementing with 10 mM $NaHCO_3$ and 10 mM 4-(2-hydroxyethyl)-1-piperazineethanesulfonic acid (HEPES; Sigma-Aldrich, St. Louis, MO, USA), are added and this medium is complemented with100 IU/mL penicillin (Merck, Merck KGaA, Darmstadt, Germany). The cells are incubated at 37 °C under an atmosphere of 95% air-5% CO_2 during 18 to 24 h until electrophysiological recording.

3.3. Electrophysiological Recording and Data Analysis

Neurons of the dorsal root ganglia are identified under a phase contrast microscope (Nikon TMS, Tokyo, Japan) and classical patch clamp methods are used for electrophysiological recordings [42]. Patch clamp pipettes are pulled from borosilicate glass capillaries using a Flaming-Brown (80/PC; Sutter Instruments, San Rafael, CA, USA). Commonly, these pipettes had a resistance of 1 to 3.5 MΩ and the seal resistance to cell membrane exceeded 1 GΩ. We used a voltage clamp amplifier Axopatch 200B (Molecular Devices, Sunnyvale, CA, USA). Command signals and data acquisition are generated by an analog-digital converter (Digidata 1200, Molecular Devices), which is controlled by the pClamp 10 software (Molecular Devices) [43]. Both voltage and current clamp experiments are performed. In these experiments, cell capacitance and series resistance are electronically compensated (80%) when the whole-cell configuration is obtained. Electrophysiological signals are low-pass-filtered at 5 or 2 kHz and digitized at 20 or 10 kHz. Cells are bathed with standard external and internal solutions, as shown in Table 4. In addition, internal solutions contain both 2 mM ATP-Mg and 1 mM GTP-Na. The pH levels of the external and internal solutions are adjusted at 7.4 with NaOH and 7.2 with KOH, respectively. Osmolarity is monitored by a vapor pressure osmometer (Wescor, Logan, UT, USA), which is adjusted with dextrose at 300 mOsm and 310 mOsm for internal and external solutions, respectively.

Table 4. Composition of standard solutions (in mM).

Solution	NaCl	KCl	$CaCl_2$	$MgCl_2$	HEPES	EGTA *
External	140	5.4	1.8	1.2	10	–
Internal	10	135	0.134	5	5	10

EGTA *—ethylene glycol tetraacetic acid.

For voltage clamp recordings, the cells are held at a holding potential of −60 mV (resting membrane potential), in where membrane currents are caused by voltage variation. The voltage shift is obtained using 10 mV voltage steps from −100 to 50 mV with duration of 800 ms, followed by a constant voltage of 20 mV during 200 ms. Thus, total membrane ionic current is recorded and the inward and outward currents are gave rise to a cell excitability and action potential generation.

For the current clamp experiments, the filters are open to 10 kHz and the pClamp software [43] generated square current pulses from −0.5 to 0.5 nA with 0.1 nA steps and 100 ms. The characteristics of the action potentials, caused by 1 ms suprathreshold pulses, are analyzed off-line using Clampfit (Molecular Devices) and Origin 8.0 (Microcal Software, Northampton, MA, USA). The phase-plane graphic of the cell voltage is obtained by plotting the first derivative of the membrane voltage (V) with

respect to time (*t*) *versus* the membrane voltage [44]. The threshold of the action potential is the voltage at which whose d*V*/d*t* increases suddenly, and action potential amplitude is the voltage difference between the maximum peak and resting potential. The duration of the action potential at 50% is defined as the duration of the action potential measured at the half of its amplitude. The maximum depolarization and repolarization rate are obtained from the phase-plane graphic as the maximum and minimum d*V*/d*t* values, respectively. The after-hyperpolarization (AHP) is defined as the potential difference between the minimum voltage value after the action potential and the membrane potential preceding the action potential. All results are reported as the mean ± standard error. For all comparisons between the control glass and TiO_2 thin film surfaces a Student's *t*-test was used, considering as significant a $p < 0.05$.

4. Conclusions

TiO_2 thin films deposited by magnetron sputtering at room temperature and annealed with different temperatures (100, 300, 500, 800 and 1100 °C) were studied, analyzing their morphology and biocompatibility. The XRD patterns showed the transition of the anatase phase to rutile phase. To evaluate the biocompatibility *in vitro* of the TiO_2 thin films, primary cultures of dorsal root ganglia (DRG) neurons were performed, evaluating their survival rate and electrophysiological activity. As a biological system, DRG neurons were selected because their normal functional electrical activity in the materials can be parametrically defined, which is a clear indication of biocompatibility. The electrophysiological recordings showed that the DRG neurons can be maintained in culture during 24 h on TiO_2 thin films surfaces. The electrophysiological properties of the neurons, indicated the cells viability and showed that they are functionally similar to those deposited on the control substrate. In the TiO_2 thin films at 800 °C, the currents amplitudes were similar to those measured on control substrate. At this temperature, the TiO_2 thin films has morphological characteristics that could create an environment adequate for the cells due to the fact that they presented a normal set of membrane ionic channels. The result of these experiments confirmed the feasibility of using TiO_2 thin films as a biocompatible material for the stimulation and recording of electrical activity of DRG neurons in culture.

Future work will include the deposition of TiO_2 thin films on the microelectrodes surface and the readout circuit to fabricate CMOS-MEMS devices. This circuit will allow recording of other parameters of biological relevance such as micropotentials due to pH.

Acknowledgments

The work was supported by National Council of Science and Technology of México (CONACyT) grants Nos. 48757 and 205190, "Programa Institucional de Fortalecimiento al Posgrado" (PIFI) and "Red del Programa de Mejoramiento del Posgrado" (PROMEP-RED) "Instrumentación de Sensores para aplicación en Fisiología y Biomedicina", "Materiales Nanoestructurados" grants from Secretaria de Educación Pública and grant "DITCo2014-01" from Centro Universitario de Vinculación y Transferencia de Tecnología de la Benemérita Universidad Autónoma de Puebla (BUAP) to Enrique Soto.

Author Contributions

Francisco López-Huerta, Agustín L. Herrera-May, Julián Hernández-Torres and Leandro García-González prepared and characterized the TiO_2 films; Blanca Cervantes and Octavio González realized the voltage clamp experiments; Blanca Cervantes, Rosario Vega and Enrique Soto analyzed the voltage clamp experiments and prepared the figures; Francisco López-Huerta, Agustín L. Herrera-May, Blanca Cervantes, Rosario Vega and Enrique Soto written and corrected the paper.

Conflicts of Interest

The authors declare no conflict of interest.

References

1. Juárez-Aguirre, R.; Domínguez-Nicolás, S.M.; Manjarrez, E.; Tapia, J.A.; Figueras, E.; Vázquez-Leal, H.; Aguilera-Cortés, L.A.; Herrera-May, A.L. Digital signal processing by virtual instrumentation of a MEMS magnetic field sensor for biomedical applications. *Sensors* **2013**, *13*, 15068–15084.
2. López-Huerta, F.; Woo-Garcia, R.M.; Lara-Castro, M.; Estrada-López, J.J.; Herrera-May, A.L. An integrated ISFET pH microsensor on a CMOS standard process. *J. Sens. Technol.* **2013**, *3*, 57–62.
3. Heredia, A.; Ambrosio, R.; Moreno, M.; Zuñiga, C.; Jiménez, A.; Monfil, K.; de la Hidalga, J. Thin film membrane based on a-SiGe: B and MEMS technology for application in cochlear implants. *J. Non Cryst. Solids* **2012**, *358*, 2331–2335.
4. Kim, J.W.; Takao, H.; Sawada, K.; Ishida, M. Integrated inductors for RF transmitters in CMOS/MEMS smart microsensor systems. *Sensors* **2007**, *7*, 1387–1398.
5. Chang, C.I.; Tsai, M.H.; Liu, Y.C.; Sun, C.M.; Fang, W. Pick-and-place process for sensitivity improvement of the capacitive type CMOS MEMS 2-axis tilt sensor. *J. Micromech. Microeng*. **2013**, *23*, doi:10.1088/0960-1317/23/9/095029.
6. Frewin, C.L.; Oliveros, A.; Weeber, E.; Saddow, S.E. AFM and cell staining to assess the *in vitro* biocompatibility of opaque surfaces. In *Atomic Force Microscopy Investigations into Biology From Cell to Protein*; Frewin, C.L., Ed.; Intech: Rijeka, Croatia, 2012; Volume 1, pp. 297–324.
7. Williams, D.F. On the mechanisms of biocompatibility. *Biomaterials* **2008**, *29*, 2941–2953.
8. *Biological Evaluation of Medical Devices—Part 2: Animal Welfare Requirements*; ISO 10993–2:2006; International Organization for Standardization: Geneva, Switzerland, 2010.
9. Soto, E.; Limón, A.; Ortega, A.; Vega, R. Características morfológicas y electrofisiológicas de las neuronas del ganglio vestibular en cultivo. *Gac. Med. Mex*. **2002**, *138*, 1–13. (In Spanish)
10. Diaz, G.; Melis, M.; Musinu, A.; Piludu, M.; Piras, M.; Falchi, A.M. Localization of MTT formazan in lipid droplets. An alternative hypothesis about the nature of formazan granules and aggregates. *Eur. J. Chem.* **2007**, *51*, 213–218.
11. Stadler, A. Transparent conducting oxides-an up-to date overview. *Materials* **2012**, *5*, 661–683.
12. Zaleska, A. Doped-TiO_2: A review. *Recent Pat. Eng.* **2008**, *2*, 157–164.

13. Casaletto, M.P.; Ingo, G.M.; Kacilius, S.; Mattongo, G.; Pandolfi, L.; Scavia, G. Surface studies of *in vitro* biocompatibility of titanium oxide coatings. *Appl. Surf. Sci.* **2001**, *172*, 167–177.
14. Niinomi, M. Biologically and mechanically biocompatible titanium alloys. *Mater. Trans*. **2008**, *49*, 2170–2178.
15. Elias, C.N.; Lima, J.H.C.; Valiev, R.; Meyers, M.A. Biomedical applications of titanium and its alloys. *J. Miner. Met. Mater. Soc.* **2008**, *60*, 46–49.
16. Okazaki, Y. On the effects of hot forging and hot rolling on the microstructural development and mechanical response of a biocompatible Ti alloy. *Materials* **2012**, *5*, 1439–11461.
17. Li, L.H.; Kim, H.W.; Lee, S.H.; Kong, Y.M.; Kim, H.E. Biocompatibility of titanium implants modified by microarc oxidation and hydroxyapatite coating. *J. Biomed. Mater. Res*. **2005**, *73A*, 48–54.
18. Izman, S.; Abdul-Kadir, M.R.; Anwar, M.; Nazim, E.M.; Rosliza, R.; Shah, A.; Hassan, M.A. Surface modification techniques for biomedical grade of titanium alloys: Oxidation, carburization and ion implant processes. In T*itanium Alloys-Towards Achieving Enhanced Properties for Diversified Applications*; Nurul, A.A.K.M., Ed.; Intech: Rijeka, Croatia, 2012; Volume 1, pp. 201–228.
19. Kim, H.; Choi, S.H.; Ryu, J.J.; Koh, S.Y.; Park, J.H.; Lee, I.S. The biocompatibility of SLA-treated titanium implants. *Biomed. Mater*. **2008**, *3*, doi:10.1088/1748-6041/3/2/025011.
20. Cai, Q.; Paulose, M.; Varghese, O.K.; Grimes, C.A. The effect of electrolyte composition on the fabrication of self-organized titanium oxide nanotube arrays by anodic oxidation. *J. Mater. Res*. **2005**, *20*, 230–235.
21. Kim, M.J.; Lim, H.J.; Lee, B.G.; Kim, J.H.; Choi, J.; Kang, J.G. Establishment of validation methods to test the biocompatibility of titanium dioxide. *Bull. Korean Chem. Soc.* **2013**, *34*, 1857–1863.
22. Kumari, T.V.; Usha, V.; Anil, K.; Bindu, M. Cell surface interactions in the study of biocompatibility. *Trends Biomater. Artif. Organs* **2002**, *15*, 37–41.
23. Sangeetha, S.; Kathyayini, S.R.; Dhivya, P.; Sridharan, M. Biocompatibility studies on TiO_2 coated Ti surface. In Proceedings of the International Conference on Advanced Nanomaterials and Emerging Engineering Technologies, Chennai, India, 24–26 July 2013.
24. Yin, Z.F.; Wu, L.; Yang, H.G.; Su, Y.H. Recent progress in biomedical applications of titanium dioxide. *Phys. Chem. Chem. Phys*. **2013**, *15*, 4844–4858.
25. Thurn, K.T.; Paunesku, T.; Wu, A.; Brown, E.M.B.; Lai, B.; Vogt, S.; Maser, J.; Aslam, M.; Dravid, V.; Bergan, R.; *et al*. Labeling TiO_2 nanoparticles with dyes for optical fluorescence microscopy and determination of TiO_2-DNA nanoconjugate stability. *Small* **2009**, *5*, 1318–1325.
26. Arbiol, A.; Cerdà, J.; Dezanneau, G.; Cirera, A.; Peiró, F.; Cornet, A.; Morante, J.R. Effects of Nb doping on the TiO_2 anatase-to-rutile phase transistion. *J. Appl. Phys*. **2002**, *92*, 853–861.
27. Senain, I.; Nayan, N.; Saim, H. Structural and Electrical Properties of TiO_2 Thin Film Derived from Sol-gel Method using Titanium (IV) Butoxide. *Int. J. Integr. Eng*. **2010**, *4*, 29–35.
28. Habijan, T.; de Miranda, R.L.; Zamponi, C.; Quandt, E.; Greulich, C.; Schildhauer, T.A.; Köller, M. The biocompatibility and mechanical properties of cylindrical NiTi films produced by magnetron sputtering. *Mater. Sci. Eng. C* **2012**, *32*, 2523–2528.
29. Tsyganov, I.A.; Maitz, M.F.; Richter, E.; Reuther, H.; Mashina, A.I.; Rustichelli, F. Hemocompatibility of titanium-based coatings prepared by metal plasma immersion ion implantation and deposition. *Nucl. Instrum. Methods Phys. Res. B* **2007**, *257*, 122–127.

30. Mändl, S. Increased biocompatibility and bioactivity after energetic PVD surface treatments. *Materials* **2009**, *2*, 1341–1387.
31. Rickert, D.; Lendlein, A.; Peters, I.; Moses, M.A.; Franke, R.P. Biocompatilility testing of novel multifunctional polymeric biomaterials for tissue engineering applications in head and neck surgery: An overview. *Eur. Arch. Otorhinolaryngol*. **2006**, *263*, 215–222.
32. Malich, G.; Markovic, B.; Winder, C. The sensitivity and specificity of the MTS tetrazolium assay for detecting the *in vitro* cytotoxicity of 20 chemicals using human cell lines. *Toxicology* **1997**, *124*, 179–192.
33. Onuki, Y.; Bhardwaj, U.; Papadimitrakopoulos, F.; Burgess, D.J. A review of the biocompatibility of implantable devices: Current challenges to overcome foreign body response. *J. Diabetes Sci. Technol*. **2008**, *2*, 1003–1015.
34. López-Huerta, F.; Herrera-May, A.L.; Estrada-López, J.J.; Zuñiga-Islas, C.; Cervantes-Sanchez, B.; Soto, E.; Soto-Cruz, B.S. Alternative post-processing on a CMOS chip to fabricate a planar microelectrode array. *Sensors* **2011**, *11*, 10940–10957.
35. Wassum, K.M.; Tolosa, V.M.; Wang, J.; Walker, E.; Monbouquette, H.G.; Maidment, N.T. Silicon wafer-based platinum microelectrode array biosensor for near real-time measurement of glutamate *in vivo*. *Sensors* **2008**, *8*, 5023–5036.
36. Seker, E.; Berdichevsky, Y.; Begley, R.M.; Reed, M.L.; Staley, K.J.; Yarmush, M.L. The fabrication of low-impedance nanoporous gold multiple-electrode arrays for neural electrophysiology studies. *Nanotechnology* **2010**, *21*, 1–7.
37. Kirkpatrick, C.J.; Peters, K.; Hermanns, M.I.; Bittinger, F.; Krump, K.V.; Fuchs, S.; Unger, R.E. *In vitro* methodologies to evaluate biocompatibility: Status quo and perspective. *ITBM RBM* **2005**, *26*, 192–199.
38. *Standard X-Ray Diffraction Powder Patterns*; Monograph 25; U.S. Department of Commerce, National Bureau of Standards: Washington, DC, USA, 1969.
39. Legrand, C.; Deville, J. Sur les parametres cristallins du rutile et de l' anatase. *C. R. Hebd Seances Acad. Sci*. **1953**, 236, 944–946. (In French)
40. McKeehan, M.; Warren, B.E. X-ray study of cold work in thoriated tungsten. *J. Appl. Phys*. **1953**, *24*, 52–56.
41. *Especificaciones Técnicas Para la Producción, Cuidado y uso de Animales de Laboratorio*; Norma Oficial Mexicana, NOM -062-ZOO-1999; Diario Oficial de la Federación: Ciudad de Mexico, Mexico, 1999. (In Spanish)
42. Hamill, O.P.; Marty, A.; Neher, E.; Sakmann, B.; Sigworth, F.J. Improved patch clamp technique for high resolution current recording from cell and cell free membrane patches. *Pflügers Arch*. **1981**, *391*, 85–100.
43. Axon™ pCLAMP® Electrophysiology Data Acquisition & Analysis Software. Molecular Devices Corporation: Sunnyvale, California, 2010.
44. Bean, B.P. The action potential in mammalian central neurons. *Nat. Rev. Neurosci*. **2007**, *8*, 451–461.